ACS NANO
Cite This: ACS Nano 2018, 12, 10231−10239
www.acsnano.org

ARTICLE

Unraveling the Origin of Operational Instability of Quantum Dot Based Light-Emitting Diodes

Jun Hyuk Chang,[†] Philip Park,[‡] Heeyoung Jung,[§] Byeong Guk Jeong,[∥] Donghyo Hahm,[†] Gabriel Nagamine,[⊥] Jongkuk Ko,[#] Jinhan Cho,[#] Lazaro A. Padilha,[⊥] Doh C. Lee,[∥] Changhee Lee,[§] Kookheon Char,*[,†] and Wan Ki Bae*[,¶]

[†]School of Chemical and Biological Engineering, Seoul National University, Seoul 08826, Korea
[‡]Department of Chemistry and Biochemistry, University of California, Los Angeles, California 90095, United States
[§]School of Electrical and Computer Engineering, Inter-University Semiconductor Research Center, Seoul National University, Seoul 08826, Korea
[∥]Department of Chemical and Biomolecular Engineering, KAIST Institute for the NanoCentury, Korea Advanced Institute of Science and Technology (KAIST), Daejeon 34141, Korea
[⊥]Instituto de Fisica "Gleb Wataghin", Universidade Estadual de Campinas, UNICAMP, P.O. Box 6165, 13083-859 Campinas, São Paulo, Brazil
[#]Department of Chemical and Biological Engineering, Korea University, Seoul 02841, Korea
[¶]SKKU Advanced Institute of Nanotechnology (SAINT), Sungkyunkwan University, Suwon-si, Gyeonggi-do 16419, Korea

Supporting Information

ABSTRACT: **We investigate the operational instability of quantum dot (QD)-based light-emitting diodes (QLEDs). Spectroscopic analysis on the QD emissive layer within devices in chorus with the optoelectronic and electrical characteristics of devices discloses that the device efficiency of QLEDs under operation is indeed deteriorated by two main mechanisms. The first is the luminance efficiency drop of the QD emissive layer in the running devices owing to the accumulation of excess electrons in the QDs, which escalates the possibility of nonradiative Auger recombination processes in the QDs. The other is the electron leakage toward hole transport layers (HTLs) that accompanies irreversible physical damage to the HTL by creating nonradiative recombination centers. These processes are distinguishable in terms of the time scale and the reversibility, but both stem from a single origin, the discrepancy between electron *versus* hole injection rates into QDs. Based on experimental and calculation results, we propose mechanistic models for the operation of QLEDs in individual quantum dot levels and their degradation during operation and offer rational guidelines that promise the realization of high-performance QLEDs with proven operational stability.**

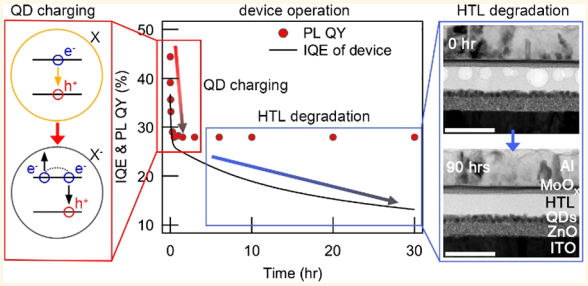

KEYWORDS: *quantum dot based light-emitting diodes, operational stability, charge injection balance, Auger recombination, degradation of organic hole transport layer*

Nanocrystal quantum dots (QDs) exhibit broad absorption but narrow emission spectral bandwidth, size-dependent emission tunability over the entire visible region, and near-unity luminescence quantum yield.[1,2] Accompanied by the capability of cost-effective solution processing, these advantageous features of QDs promote their use in a variety of light-emitting systems.[3−17] Among potential applications, QD-based light-emitting diodes (QLEDs),[3,8−17] in which electrically injected charge carriers recombine to emit photons, have received particular interest as next-generation displays due to their excellence in color gamut, brightness, and efficiency. Since the first demonstration,[3] the research area of QLEDs has witnessed a tremendous amount of progress in the last two decades with respect to the external

Received: May 5, 2018
Accepted: October 10, 2018
Published: October 10, 2018

DOI: 10.1021/acsnano.8b03386
ACS Nano 2018, 12, 10231−10239

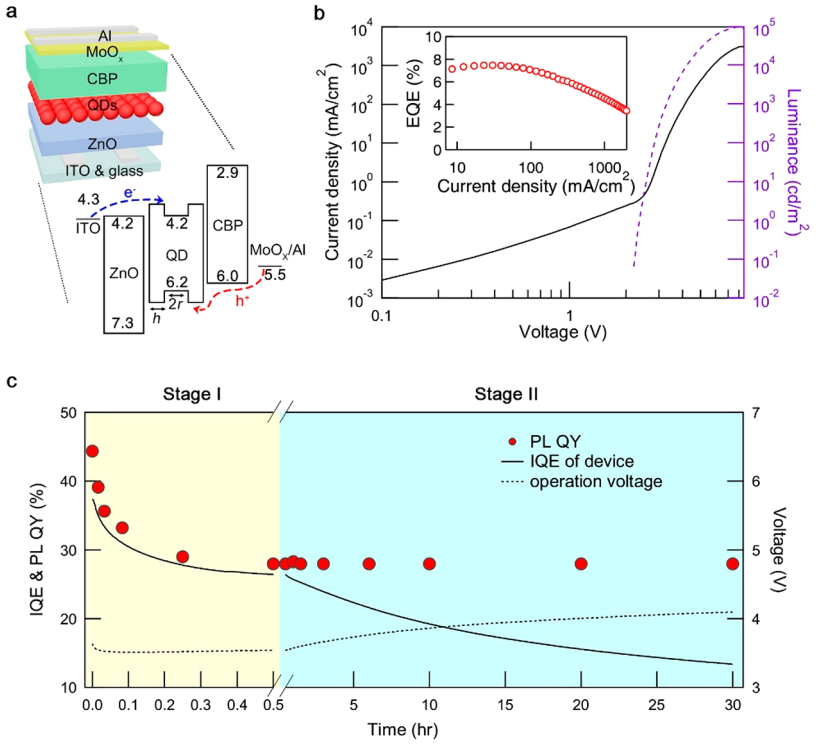

Figure 1. Representative characteristics of QLED investigated in the present study. (a) Schematic illustration (top left) and the energy band diagram (bottom right) and (b) current density (J)−voltage (V)−luminance characteristics (L) (inset: external quantum efficiency (EQE) *versus* J) of an inverted QLED imploying CdSe(radius (r) = 2 nm)/$Zn_{0.5}Cd_{0.5}S$(thickness (h) = 6.3 nm) type I core/shell heterostructured QDs. (c) Operation time-dependent traces of the internal quantum efficiency (IQE, black solid line) and the operation voltage (black broken line) of a QLED under a current density of 30 mA/cm^2 (black solide line) and the phololuminescence quantum yield (PL QY) of the QD emissive layer in the corresponding device (red filled circle).

quantum efficiency (EQE) and brightness, satisfying requirements for use in light-emitting devices.[10,12−14,16,18]

Stable operation of QLEDs at desired brightness is essential for their practicable use in displays and lightings. Despite substantial progress made in the device performance, the state-of-the-art QLEDs still suffer from poor operational stability. For instance, even QLEDs with a peak efficiency close to the theoretical limit (*i.e.*, EQE ≈ 20%) show an abrupt drop of luminance efficiency during operation (50% decrease in the luminance efficiency from the initial luminance after 2 h of operation).[12] Nevertheless, understanding the origin of the operational instability of QLEDs is lagging behind, which in turn limits advancement of QLEDs toward commercialization.

Herein, we explore the origin of operational instability of QLEDs with organic/inorganic hybrid charge transport layers (CTLs). We conduct a comprehensive study across electrical and optoelectronic characterization of QLEDs under operation and spectroscopic analysis of the QD emissive layer in corresponding devices. On the basis of the experimental and calculation results, we construct a mechanistic model for the operation of QLEDs in individual quantum dot levels and their degradation during operation. At the end, we discuss a practical strategy for the realization of high-performance QLEDs with proven operational stability.

RESULTS AND DISCUSSION

QLEDs consist of multiple layers of functional materials that are potentially responsible for the operational instability of devices. To avoid unwanted complications that originate from the materials' intrinsic instability, we have conducted an operational stability test on QLEDs that employ materials with proven performance and stability. Specifically, as light-emitting materials we have chosen CdSe(radius (r) = 2.0 nm)/$Zn_{0.5}Cd_{0.5}S$(thickness (h) = 2.5, 3.0, 4.5, and 6.3 nm) type I core/shell heterostructured QDs[14] (PL QYs ≈ 80%) and CdSe(r = 2.0 nm)/CdS(h = 5.5 nm) quasi-type II core/shell heterostructured QDs (PL QY = 50%),[11,17,19] whose photophysical properties are extensively understood (Figure S1, Table S1). An inverted QLED that employs a 40 nm thick ZnO nanoparticle film and 60 nm thick 4,4′-bis(*N*-carbazolyl)-1,1′-bipheny (CBP) as electron transport layer (ETL) and hole transport layer (HTL) is used as the device platform (Figure 1a). In such a device configuration, electrons and holes drift from ZnO//ITO and CBP//MoO_X//Al, respectively, and recombine within the QD emissive layer to yield photons. The fabricated QLED employing CdSe(r = 2.0 nm)/$Zn_{0.5}Cd_{0.5}S$(h = 6.3 nm) QDs exhibits a turn-on voltage as low as the optical bandgap of QDs (2.2 eV), a peak EQE of 7.48%, and a peak brightness over 100 000 cd/m^2 (Figure 1b).

We characterized the operational stability of QLEDs by monitoring the time-dependent change in the device characteristics (*e.g.*, luminance (L), voltage (V), and efficiency) under the constant current density operation. To examine the relationship between the luminance efficiency of the QD emissive layer and the device efficiency, we compared photoluminescence quantum yields (PL QYs) of the QD emissive layers over time with internal quantum efficiencies (IQEs) of the devices. The absolute PL QY of the QD emissive films before operation is measured to be 44%. The discrepancy between PL QYs of solution samples (~80%) and the film

DOI: 10.1021/acsnano.8b03386
ACS Nano 2018, 12, 10231−10239

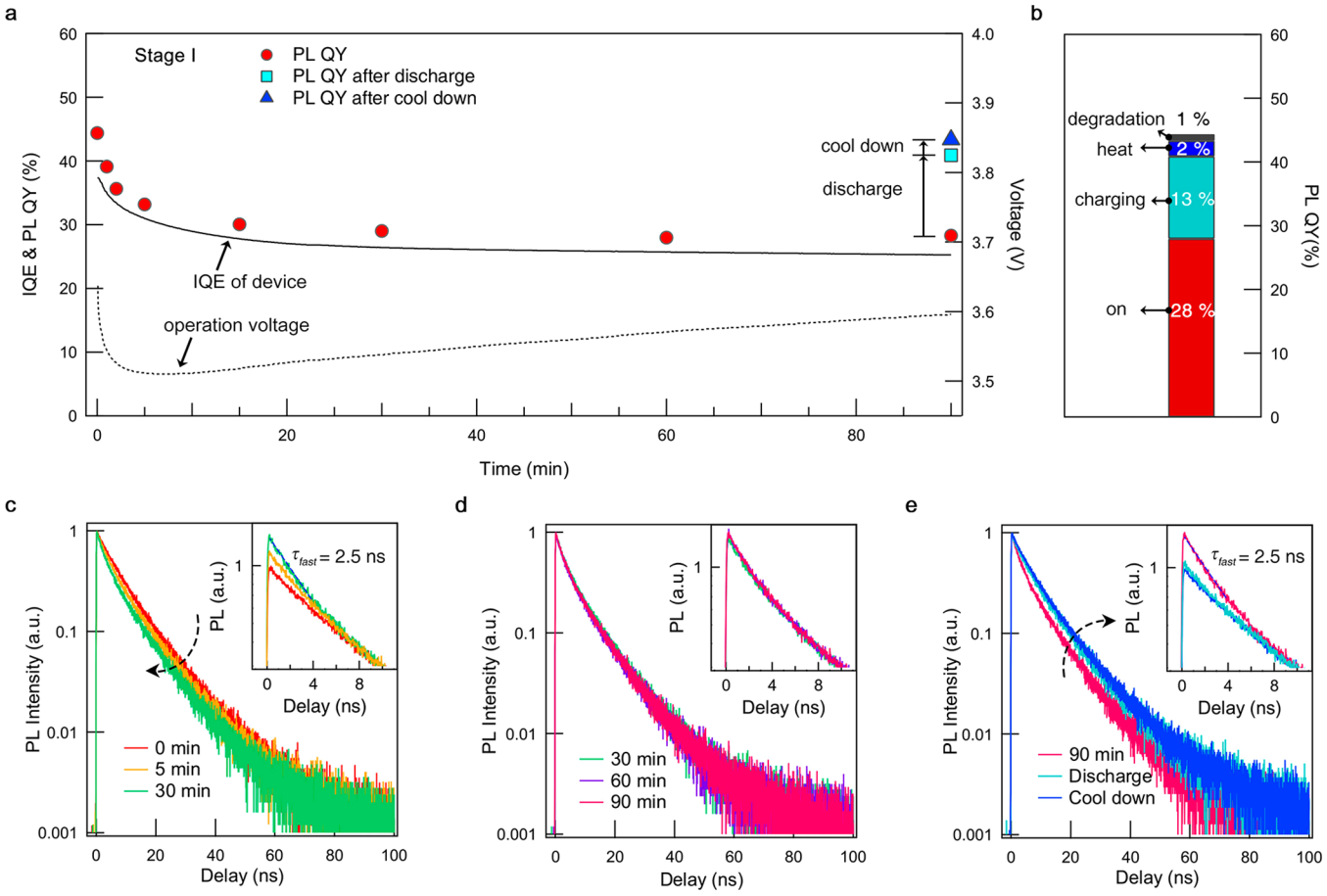

Figure 2. Changes in optical characteristics of the QD emissive layer under the device operation. (a) Operation time-dependent traces of IQE (black solid line) and the operation voltage (black broken line) of the QLED employing CdSe(r = 2.0 nm)/$Zn_{0.5}Cd_{0.5}S$(h = 6.3 nm) QDs under continuing operation at a current density of 30 mA/cm^2 and PL QY (red cirlce) of the QD emissive film in the corresponding device. PL QYs of the QD emissive layer in 90 min-operated QLED after applying reverse voltage (−7 V, cyan square) and additional cooling for 1 h (blue triangle) are overlaid for comparison. (b) Contributions of charging, heat, and the permanent degradation of QDs to the reduction of luminescence efficiency of the QD emissive layer in a 90 min-operated QLED. Normalized PL decay curves of the QD emissive layer (c, d) after operation for 0, 5, 30, 60, and 90 min and (e) after applying reverse voltage (−7 V, cyan) and cooling for 1 h (blue) (insets: PL decay curves normalized with the PL intensities at 10 ns of time delay).

(44%) is attributed to the energy transfer processes among adjacent QDs in films that escalate the probability of nonradiation recombination processes for excitons.[14] IQEs are estimated from EQEs on the basis that the out-coupling efficiency of the current device structure is approximately 0.2 in the chosen device architecture. Figure 1c displays device efficiencies and PL QYs of the QD emissive layer under operation at the current density of 30 mA/cm^2 (L_0 = 2400 cd/m^2). The device efficiency falls rapidly from its initial value during the early device operation and continues to decrease gradually under operation. By contrast, the PL QY of the QD emissive film remains unchanged after the sudden decrease during the early device operation. Interestingly, the tendency observed in PL QYs of the QD emissive film match that of the device efficiencies during the early decay stage (stage I), indicating that the initial rapid drop of the device efficiency is related to the luminescence efficiency loss of the QD emissive layer.

To identify the origin of PL QY loss of the QD emissive layer during device operation, we conducted photophysical characterization on the QD emissive layer in the early decay stage (Figure 2). PL QY of the QD emissive film decreases by 37% from its initial value in 30 min of operation at a current density of 30 mA/cm^2 (Figure 2a,b). Time-correlated single photon counting (TCSPC) measurement on the QD emissive layer clearly demonstrates that PL QY loss accompanies the rise of fast decay components (Figure 2c), implying that fast nonradiative recombination pathways emerge in the QD emissive layer during the early operation stage. Once the development of fast decay is complete, noticeable change in the QD emissive layer is not observed upon continuing operation (Figure 2d). Surprisingly, the time scale of the fast decay component (*ca.* 2.5 ns) agrees well with the negative trion (two electrons and one hole, X^-) lifetime of QDs obtained from comparison between PL decay under the static and stirred conditions (*ca.* 2.7 ns, Figure S2).[19−21] This demonstrates that the fast nonradiative decay pathways originate from the accumulation of excess electrons in QDs during the device operation, which escalates the probability for the nonradiative Auger recombination processes.[11,22,23]

To validate the idea that the early stage loss originates from the charge accumulation in the QD emissive layer, we have applied reverse bias through the QLED to extract excess electrons and neutralize QDs. After applying reverse bias (−7 V), the fast decay component disappears (Figure 2e) and the PL QY of the QD emissive layer recovers to 93% of its initial

DOI: 10.1021/acsnano.8b03386
ACS Nano 2018, 12, 10231−10239

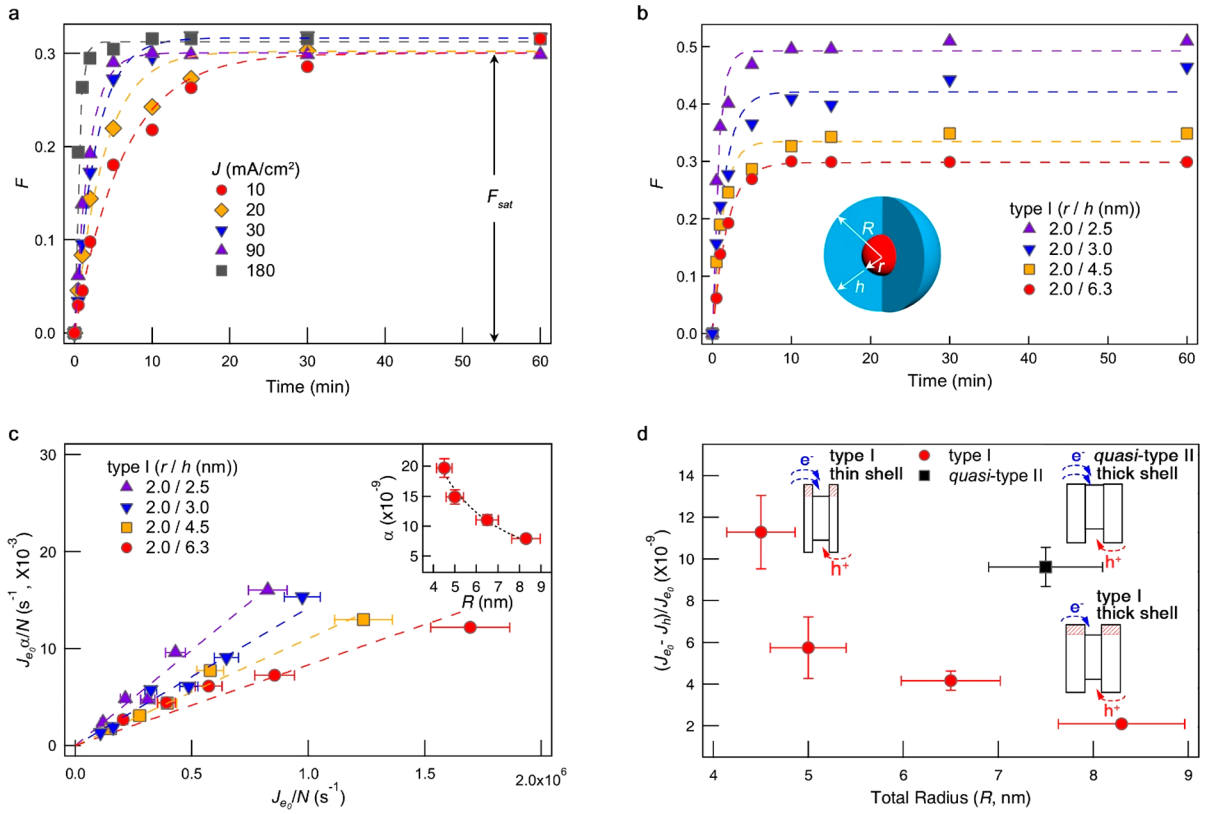

Figure 3. Influence of the structural formulations of QDs on the early efficiency drop in QLEDs. Operation time-dependent traces of the fraction of charged QDs (F) in the QD emissive layer of (a) QLEDs implementing CdSe(r = 2.0 nm)/$Zn_{0.5}Cd_{0.5}S$(h = 6.3 nm) type I QDs under the current densities of 10, 20, 30, 90, and 180 mA/cm^2 and (b) QLEDs implementing CdSe(r = 2.0 nm)/$Zn_{0.5}Cd_{0.5}S$ type I QDs with varying shell thicknesses (h = 2.5, 3.0, 4.5, and 6.3 nm) operated under similar charge carrier injection rate per individual dots ($\frac{J}{N} \cong 10^6$/s per dot). (c) Repulsion rate per dot ($\frac{J_e(0)\alpha}{N}$) versus initial electron injection rate per dot ($\frac{J_e(0)}{N}$) in QLEDs implementing CdSe(r = 2.0 nm)/$Zn_{0.5}Cd_{0.5}S$ type I QDs with varying shell thicknesses (h = 2.5, 3.0, 4.5, and 6.3 nm) (inset: the repulsion coefficient (α) as a function of the total radius (R, $R = r + h$) of type I QDs). (d) Initial charge injection imbalance ($\frac{J_e(0) - J_h}{J_e(0)}$) in QLEDs employing QDs with varying structural formulations (*i.e.*, CdSe(r = 2.0 nm)/$Zn_{0.5}Cd_{0.5}S$(h = 2.5, 3.0, 4.5, and 6.3 nm) type I QDs (red circle) and CdSe(r = 2.0 nm)/CdS(h = 5.5 nm) quasi-type II QDs (black square)).

value (Figure 2a,b). The series of experiments coherently attest that PL QY loss in the QD emissive layer mainly originates from the accumulation of excess electrons in QDs during device operation that promotes nonradiative Auger recombination of injected charge carriers. Near-complete recovery of PL QY of the QD emissive layer (~98% of the initial value) is observed after 1 h of cooling, signifying that PL QY loss of the QD emissive layer is in part contributed by the heat generated during device operation. We attribute minor but apparent PL QY loss (1−2%) of the QD emissive layer to the permanent degradation of QDs under the device operation condition.

The lowest quantized state of the conduction band ($1S_e$) of CdSe QDs (4.2 eV) resides close to the conduction band edge (CBE) energy level of ZnO (4.2 eV), and thus electrons readily migrate from ITO//ZnO into QDs (Figure 1a, Figure S4). By contrast, the hole injection from CBP into QDs is largely hindered by the energy level offset (0.2 eV) between the lowest quantized state of the valence band ($1S_h$) of CdSe QDs (6.2 eV) and the highest occupied molecular orbital (HOMO) of CBP (6.0 eV). The asymmetry in charge injection rates readily yields accumulation of excess electrons within QDs that promotes the probability of nonradiative Auger recombination processes. The fraction of negatively charged QDs within the QD emissive layer increases during the early operation stage, which in turn leads to the decrease in the luminescence efficiency of the QD emissive layer and thereby the device efficiency.

The PL QY of the QD films remains unchanged after the early efficiency drop. We note that this trend is not a particular event but generally observed in QLEDs regardless of the operation conditions (Figure 3a), the structural formulation of QDs (Figure 3b), or other references (Figure S6). Spectroscopic analysis corroborates that the fraction of negatively charged QDs ($F = C(t)/N$, where $C(t)$ = the number of charged QDs per unit area at time t and N = the number of QDs per unit area) reaches saturation after the early decay stage, which reflects that electron and hole injection rates into the QD emission layer equalize after the fraction of charged QDs within the emissive layer reaches a certain value (F_{sat}). The electron−hole recombination is a dominant component of overall current density and determined by the hole injection rate because the hole injection rate is inferior to its counterpart. Since the hole injection rate is fixed over time at constant current operation, the balanced charge injection rate indicates the reduction of the electron injection rate from

DOI: 10.1021/acsnano.8b03386
ACS Nano 2018, 12, 10231−10239

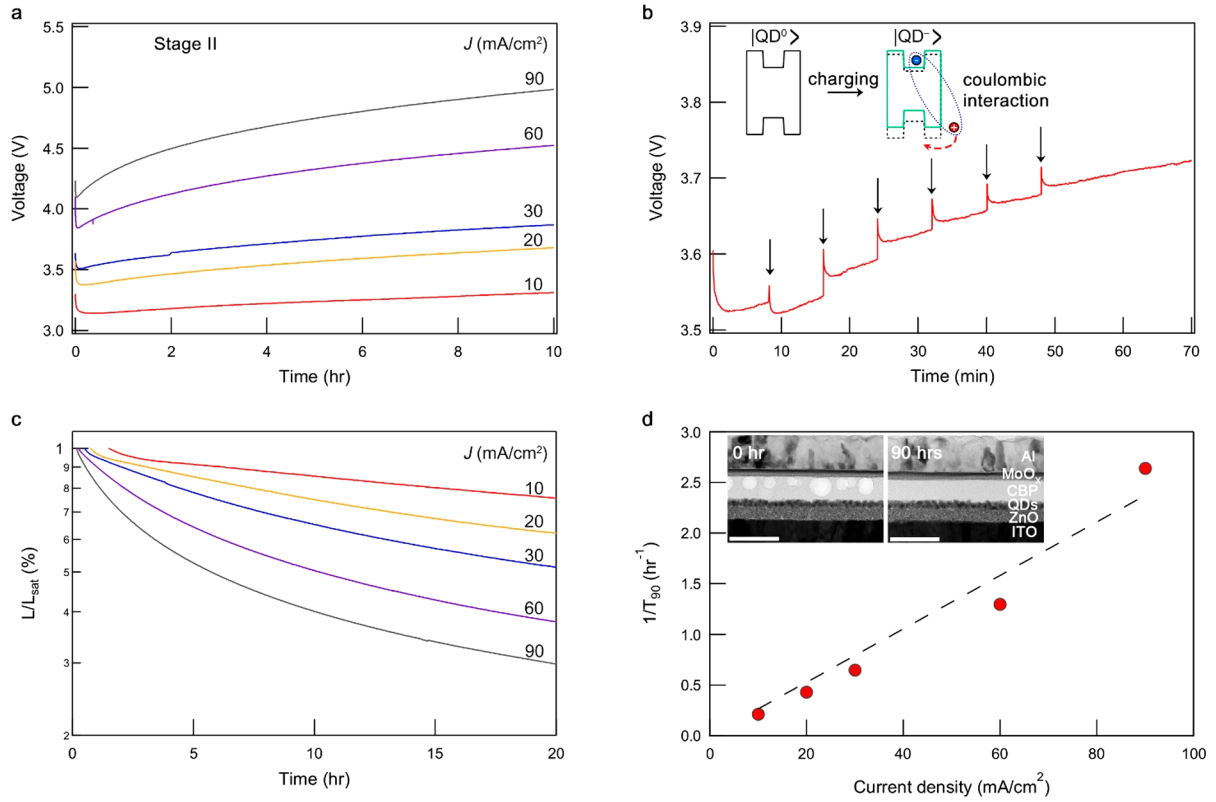

Figure 4. Electrical and optoelectronic characteristics of QLEDs under operation. Operation time-dependent traces of the operation voltage of QLEDs employing CdSe(r = 2.0 nm)/$Zn_{0.5}Cd_{0.5}S$(h = 6.3 nm) QDs (a) under constant current operation (J = 10, 20, 30, 60, and 90 mA/cm^2) and (b) under a current density of 30 mA/cm^2 with pulsed applied reverse voltage (−7 V) (signified with arrows). (c) Operation time-depdendent luminance trace of LEDs under varying current densities from 10 to 90 mA/cm^2, where the initial device efficiencies are comparable (EQE_0 = 7.00 ± 0.14%). The normalized luminance traces of devices are shown from the point (L_{sat}) where the PL QY of the QD emissive layer becomes constant. (d) Rate for the slow decay ($1/T_{90}$, where T_{90} denotes the time when the luminance become 90% of L_{sat}) as a function of the applied current density (inset: cross-sectional TEM images of devices as prepared (left) and after 90 h of operation at 30 mA/cm^2 (right); scale bar, 100 nm).

ZnO into QDs along with the accumulation of negative charges in the QD emissive layer.

To explain the saturation of PL QY loss of the QD emissive layer after the early decay, we build a model that takes into account the fact that the electron injection from ZnO ETL into QDs is hindered by the presence of excess electrons in the QD emissive layer. The fraction of charged QDs ($F(t)$) at a given time t can be expressed as below.

$$F(t) = C(t)/N = \frac{J_e(0) - J_h}{J_e(0)} \frac{1}{\alpha}\left(1 - \exp\left(-\frac{J_e(0)\alpha}{N}t\right)\right) \quad (1)$$

where $J_e(t)$ and J_h are the number of injected electrons and holes into QDs in unit area (cm^2) at time t, N is the number of QDs in unit area (cm^2), $C(t)$ is the number of charged QDs in unit area (cm^2) at time t, and α is the repulsion coefficient that hinders electron injection from the ZnO ETL into QDs (see the Supporting Information). We note that the number density of each sized QDs is obtained from TEM images and taken into account to calculate the fraction of charged QDs.

Figure 3a displays operation time-dependent traces of the fraction of negatively charged QDs ($F(t) = C/N$) in QLEDs operated at varying current densities from 10 to 180 mA/cm^2, where the initial device efficiencies are similar (EQE_0 = 7.00 ± 0.14%). For all conditions, the charging fractions (F) of QDs obtained from spectroscopic analysis fit well with eq 1, supporting the credibility of our proposed model. By modulating applied current densities, we could obtain the repulsion coefficient (α) for a series of CdSe/$Zn_{0.5}Cd_{0.5}S$ type I heterostructured QDs with varying shell thicknesses (Figure 3c) and observe that the repulsion coefficient for electrons residing in QDs and electrons in ZnO nearby QDs is inversely proportional to the total radius of the QDs ($R^{1.5}$, $R = r + h$) in type I heterostructured QDs, in which the electron and hole wave functions are strongly confined within the CdSe core phase and surrounded by the $Zn_{0.5}Cd_{0.5}S$ shell.

The multiple runs of experiments from the series of samples verify the validity of our model that the electron injection rate from ZnO into QDs is obstructed by the presence of excess electrons in CdSe emissive cores. Given that the saturated fraction of charged QDs is inversely proportional to the repulsion coefficient ($F_{sat} \propto 1/\alpha$), the use of thin-shell QDs that have a greater repulsion coefficient is expected to benefit the charge balance and thereby the operational stability. Contrary to the expectation, in the present study, QLEDs implementing thick-shell type I QDs display better operational stability than ones with thin-shell type I QDs or thick-shell quasi-type II QDs. We attribute this to the fact that a thick $Zn_{0.5}Cd_{0.5}S$ shell impedes the electron injection from ZnO into the CdSe core and helps reduce the charge injection imbalance ($\frac{J_e(0) - J_h}{J_e(0)}$) in the QD emissive layer by the extent that sufficiently compensates the penalty imposed on the repulsion coefficient

DOI: 10.1021/acsnano.8b03386
ACS Nano 2018, 12, 10231−10239

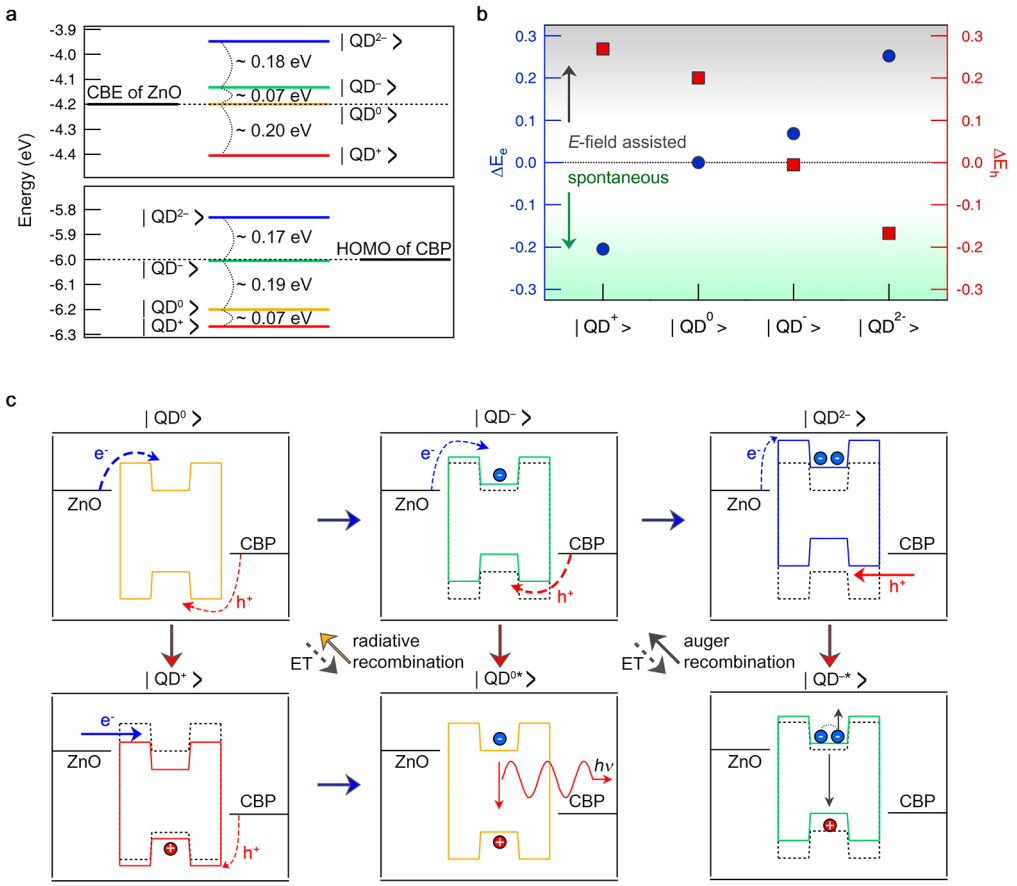

Figure 5. Mechanistic overview of QLED operation. (a) Calculated lowest quantized electronic states for an electron (up) and hole (down) of singly positively charged (QD^+), neutral (QD^0), and singly (QD^-) and doubly negatively charged QDs (QD^{2-}). (b) Energy level offsets for electron injection from the CBE energy level of ZnO into the lowest quantized electronic energy level of each charged state of QDs (ΔE_e, blue circle (left)) and hole injection from the HOMO energy level of CBP into the lowest quantized hole energy level of each charged state of QDs (ΔE_h, red square (right)) at static conditions (without external electric field). We note that the energy offsets for electron and hole injection at working devices are different from (b). (c) Sketch of the relationship among probable QD charged states in an operating QLED. Charge injection of an electron (blue arrow) and hole (red arrow), radiative recombination (yellow arrow), Auger recombination (gray arrow), charge hopping (improbable), and energy transfer (ET, broken gray arrow) are noted. The electronic energy levels of neutral QD (gray dashed line) are superimposed on that of charged QDs for comparison.

(Figure 3d). We note that the trend, the enhancement of charge injection balance in thick-shell QDs, is consistent with our previous results[11,14] and recent reports by other research groups.[7]

The presence of excess electrons in the QD emissive layer not only hinders the electron injection from the ETL into the QDs but also promotes the hole injection from the HTL into the QDs. The Coulombic attraction between excess electrons in the QDs and holes at the CBP HTL nearby the QDs is experimentally evinced with the reduction of the operation voltage at the constant current density operation (Figure 4a) and also with the increase in the operation current density at the constant applied voltage (Figure S6). Specifically, the operation voltage for applying 30 mA/cm^2 falls by 0.13 V from its initial operation voltage (3.64 V) in 5 min of operation. The reduced operation voltage recovers to the high level after discharging the QD emissive layers (Figure 4b). This validates that the hole injection from the CBP HTL into the QDs is facilitated by the presence of excess electrons.[7,24,25] The operation voltage starts to increase after the saturation of QD charging and continues to rise beyond the initial operation voltage under operation (4.43 V after 90 h operation). Since the hole injection rate is fixed over time at the constant current operation condition, the increase in the operation voltage is a result of the rise of the electrical resistivity of hole injection/transport layers (MoO_x/CBP) due to the materials' degradation of hole injection/transport layers.[26,27] We note that the increased operation voltage does not recover to its original value by applying reverse voltage or cooling.

The electron in organic HTLs is known to cause structural deformation of organic materials and create nonradiative recombination centers in HTLs.[26−30] In the present QLEDs the electron injection rate exceeds the hole injection rate, and thus electrons readily overflow toward the organic HTL, which results in permanent material degradation and in turn exacerbates the device performance as observed in the increase in the operation voltage and the reduction of the luminance efficiency of the devices. To better understand this, we conducted current-density-dependent operational stability tests on QLEDs. In order to exclude the influence of charging on the device efficiency, we plotted the luminance (device efficiency) of devices from the point (L_{sat}) where the PL QY becomes constant (Figure 4c). The rate for the slow decay ($1/T_{90}$, T_{90} denotes the time when the luminance becomes 90% of L_{sat}) is linearly proportional to the applied current densities (initial luminance) (Figure 4d). Since the device efficiencies

DOI: 10.1021/acsnano.8b03386
ACS Nano 2018, 12, 10231−10239

that are linked with the extents of charge injection balance are similar in chosen variations of the applied current density, the linear relationship between the rate for the slow decay ($1/T_{90}$) and the applied current density verifies that excess electrons that leak from the side of ITO//ZnO//QDs toward CBP are indeed responsible for the degradation of CBP that creates nonradiative recombination centers and thereby the decrease in the device efficiency. We note that the sign of HTL degradation under operation is also observed from cross-sectional TEM images of devices. A Ga^+ ion beam readily damages the organic HTL during sample preparation *via* a focused ion beam and readily leaves void marks in the as-prepared QLED (0 h operation), but these marks are not observed from the 90 h-operated one (Figure 4d (inset), Figure S7). From the comparative TEM images along with the change in the electric resistivity of devices, we speculate that the electrons in CBP decompose chemical bonds of molecules and cause the cross-linking of molecules.

The optical characteristics of the QD emissive layer and the optoelectronic properties of devices enable us to comprehend the device operation mechanism that describes the sequences of charge carrier injection into individual QDs within the operating device (Figure 5). To quantitatively evaluate the injection feasibility of the electron and hole into each charging states of QDs, we assessed the lowest quantized electronic states of QDs depending on their charging states (Figure 5a,b) by performing the quantum mechanical calculation including self-consistency and dielectric mismatch effect in three dimensions (Figure S8).[31,32] The interaction between the electrons residing in the core phase of QDs and its own imaginary charges escalates the lowest quantized electronic states for the electron and hole by 0.07 eV (0.25 eV) and 0.19 eV (0.36 eV) for singly (doubly) negatively charged QDs, respectively, as does the shell energy. Likewise, the presence of a hole in the core lowers the lowest quantized electronic states for the electron and hole by 0.20 and 0.07 eV, respectively. We note that the changes in the energy levels of charged QDs are directly linked to the repulsion coefficient (α).

The calculated energy levels of QDs at each charging state along with the experimental results enable us to outline the relationship among probable charging states of QDs under device operation (Figure 5c). Due to the larger energy barrier for hole injection than that of electron injection ($\Delta E_e - \Delta E_h = -0.20$ eV), a neutral QD is more likely to accept an electron to turn into singly negatively charged QDs ($QD^0 + e^- \rightarrow QD^-$). The hole is energetically preferred to be injected into singly negatively charged QDs than its counterpart ($\Delta E_e - \Delta E_h = 0.07$ eV), but the extent of injection rate difference is less significant than the case of neutral QDs. The majority of singly negatively charged QDs become neutralized by accepting holes ($QD^- + h^+ \rightarrow QD^0 + h\nu$), and the remainder accommodate extra electrons to change into negatively charged QDs ($QD^- + e^- \rightarrow QD^{2-}$). The ionization energy level of doubly negatively charged QDs resides higher than the HOMO of CBP ($\Delta E_h = -0.17$ eV), so that doubly negatively charged QDs spontaneously accept a hole from CBP to turn into singly negatively charged QDs after undergoing a nonradiative Auger recombination process ($QD^{2-} + h^+ \rightarrow QD^-$). Likewise, the CBE energy level of singly positively charged QDs resides lower than that of ZnO by 0.20 eV ($\Delta E_e = -0.20$ eV), and thus immediate injection of an electron takes place to neutralize singly positively charged QDs ($QD^+ + e^- \rightarrow QD^0 + h\nu$).

We note that neutral (QD^0) and singly negatively charged QDs (QD^-) are energetically stable under the unbiased condition ($V_{app} = 0$) and thereby observed with TCPSC measurement. By contrast, singly positively charged (QD^+) and doubly negatively charged QDs (QD^{2-}) spontaneously accommodate electrons and holes, respectively, and therefore these charged states are rarely monitored with TCSPC. We speculate that the presence of higher charge state QDs (*e.g.*, QD^{2+} or QD^{3-}) is unlikely in chosen device operation conditions due to the large energy barrier (>0.25 eV) for electrons (holes) to be injected into doubly negatively charged (singly positively charged) QDs.

CONCLUSION

In summary, we have identified the operational instability of QLEDs originates from the disparity between electron and hole injection rate. The charge injection imbalance causes accumulation of extra charge carriers (electrons) in the QD emissive layer that promotes nonradiative Auger recombination processes, resulting in the reduction of the luminance efficiency of the QD emissive layer and thereby the device efficiency. Simultaneously the charge injection imbalance yields the leakage of electrons toward organic HTLs that causes material degradation. The device efficiency drop by QD charging arises promptly (less than an hour) but can be recovered by extracting the extra charge carriers, whereas the gradual HTL degradation leads to the permanent deterioration of device performance.

The device degradation mechanisms are distinguishable with respect to the time scale and the reversibility, but both originate from the same origin, the disparity between electron *versus* hole injection rates into QDs. The charge injection imbalance in current QLEDs results from the large energy offset for hole injection from the HTL into QDs. The apparent next step to overcome this issue is either changing the composition of the emitters to ones whose ionization energy levels dwell close to the HOMO energy level of organic HTLs or adopting HTLs that are capable of reducing the energetic barrier for hole injection or taking a combination of both. At the same time, the development of QDs with suppressed Auger recombination[7,11,33] or chemically robust HTLs[18,34] will also enable the enhancement in device efficiency and stability of QLEDs under operation. We believe that innovating materials and optimizing device structure will result in high-efficiency and stable QLEDs, which will foster their practical uses in displays and lightings.

EXPERIMENTAL METHODS

Materials. All QD synthesis was conducted under an inert condition by using the Schlenk line technique. CdSe(r = 2 nm)/$Cd_{0.5}Zn_{0.5}S$(h = 2.5, 3.0, 4.5, and 6.3 nm) type I QDs (PL QYs ≈ 80%) and CdSe(r = 2 nm)/CdS(h = 7.5 nm) quasi-type II QDs (PL QY = 50%) were synthesized by previously reported methods.[14,19] The resultant QDs were purified five times *via* the precipitation/redispersion method and dispersed in toluene for further experiments. A ZnO nanoparticle solution was prepared *via* the sol−gel method.[11,35] CBP was purchased from OSM (Organic Semiconductor Materials). MoO_x and Al were purchased from iTASCO (Korea).

Device Fabrication and Characterization. A ZnO nanoparticle dispersion (20 mg/mL in *n*-butanol) was spun-cast on patterned ITO substrates with a spin rate of 3000 rpm for 30 s to form ZnO films. The ZnO films were then annealed at 300 °C under air for 1 h. QD dispersions (20 mg/mL in toluene) were then spun-cast onto ZnO//ITO at 4000 rpm for 30 s. CBP, MoO_x, and Al electrode layers were

DOI: 10.1021/acsnano.8b03386
ACS Nano 2018, 12, 10231−10239

thermally evaporated under a vapor pressure of 2×10^{-6} Torr onto QDs//ZnO//ITO substrates at deposition rates of 0.8−1, 0.3, and 4−5 Å·s^{-1}, respectively. The current−voltage−luminance (J−V−L) characteristics of the devices were obtained with a Keithley-236 source-measure unit, a Keithley-2000 multimeter unit coupled with a calibrated Si photodiode (Hamamatsu S5227-1010BQ), and a photomultiplier tube detector. Luminance and efficiencies of QLEDs were measured and calculated from the photocurrent data obtained with the Si photodiode. Electroluminescence spectra were obtained using a spectroradiometer (Konica Minolta CS-2000). Time-dependent J−V−L characteristics of devices were measured with an LED lifetime test system (McScience MC620S). The absolute PL QY of the QD emissive layer before operation (t = 0) was measured with the PL measurement system coupled with the integrating sphere. The time-dependent PL QYs of the QD emissive layer were estimated by comparing PL intensities of the QD emissive layer that were measured under unbiased condition (applying voltage = 0) after device operation with the initial PL intensity. We note that the PL intensity and PL decay dynamics of the QD emissive layer remain constant during the *ex situ* measurements (~3 min).

Optical Characterization. UV−vis absorption and photoluminescence spectra were obtained with a Lambda 35 spectrometer (PerkinElmer) and a Fluoromax-4 spectrometer (Horiba Science), respectively. The absolute PL QYs of film samples were obtained at an excitation wavelength of 520 nm with a C11347-01 (Hamamatsu Photonics). The measurements to characterize the PL decay dynamics were conducted with a TCSPC system from Horiba-Jovin Yvon, which has a resolution of about 100 ps. The samples were excited at 2.38 eV at a repetition rate of 200 kHz.

Modeling and Simulation. The fraction of charged QDs and the electronic injection rate at a given time are assessed by taking into account the Coulombic interactions between the charge carrier within the QD emissive layer and the charge carrier in charge transport layers. The lowest quantized electronic states of QDs are calculated by performing the quantum mechanical calculation including self-consistency and dielectric mismatch effect in three dimension (see Supporting Information).

ASSOCIATED CONTENT

Supporting Information

The Supporting Information is available free of charge on the ACS Publications website at DOI: 10.1021/acsnano.8b03386.

Detailed characteristics of QDs used in the present study; calculation of lowest quantized electronic states of charged QDs; modeling of QD charging during QLED operation; sketches of the device degradation mechanisms in QLEDs under operation; applied voltage-dependent PL QY change of the QD emissive layer within the device (PDF)

AUTHOR INFORMATION

Corresponding Authors

*E-mail (K. Char): khchar@snu.ac.kr.
*E-mail (W. K. Bae): wkbae@skku.edu.

ORCID

Heeyoung Jung: 0000-0001-6094-3498
Byeong Guk Jeong: 0000-0002-0544-364X
Jinhan Cho: 0000-0002-7097-5968
Lazaro A. Padilha: 0000-0002-8825-6611
Doh C. Lee: 0000-0002-3489-6189
Changhee Lee: 0000-0003-2800-8250
Kookheon Char: 0000-0002-7938-8022
Wan Ki Bae: 0000-0002-3832-2449

Author Contributions

W.K.B. conceived the idea. J.H.C., B.G.J., and D.H. synthesized QDs. J.H.C. and H.J. conducted device fabrication and characterization. D.H., G.N., J.K., and L.A.P. conducted photophysical characterization. P.P. performed the calculation. D.L., P.P., C.L., J.C., K.C., and W.K.B. were involved in designing the experiments, discussion of the results, and writing the manuscript.

Notes

The authors declare no competing financial interest.

ACKNOWLEDGMENTS

This work was financially supported by the Basic Science Research Program (2018R1D1A1B07047824) and Nanomaterials Technology Development Program (2016M3A7B4910620) through the National Research Foundation of Korea (NRF) funded by the Ministry of Education. K.H.C. acknowledges the Ministry of Trade, Industry & Energy (MOTIE, 10076340). G.N. and L.A.P. acknowledge the financial support from São Paulo Research Foundation - FAPESP (2013/16911-2).

REFERENCES

(1) Brus, L. Electronic Wave Functions in Semiconductor Clusters: Experiment and Theory. *J. Phys. Chem.* **1986**, *90*, 2555−2560.
(2) Klimov, V. I. *Nanocrystal Quantum Dots*; CRC Press, 2010.
(3) Colvin, V.; Schlamp, M.; Alivisatos, A. P. Light-Emitting-Diodes Made from Cadmium Selenide Nanocrystals and a Semiconducting Polymer. *Nature* **1994**, *370*, 354−357.
(4) Jang, E.; Jun, S.; Jang, H.; Lim, J.; Kim, B.; Kim, Y. White-Light-Emitting Diodes with Quantum Dot Color Converters for Display Backlights. *Adv. Mater.* **2010**, *22*, 3076−3080.
(5) Lim, J.; Jun, S.; Jang, E.; Baik, H.; Kim, H.; Cho, J. Preparation of Highly Luminescent Nanocrystals and Their Application to Light-Emitting Diodes. *Adv. Mater.* **2007**, *19*, 1927−1932.
(6) Klimov, V.; Mikhailovsky, A.; Xu, S.; Malko, A.; Hollingsworth, J.; Leatherdale, C.; Eisler, H.-J.; Bawendi, M. Optical Gain and Stimulated Emission in Nanocrystal Quantum Dots. *Science* **2000**, *290*, 314−317.
(7) Lim, J.; Park, Y.-S.; Klimov, V. I., Optical Gain in Colloidal Quantum Dots Achieved with Direct-Current Electrical Pumping. *Nat. Mater.* **2017**, *17*, 42.
(8) Coe, S.; Woo, W.-K.; Bawendi, M.; Bulović, V. Electroluminescence from Single Monolayers of Nanocrystals in Molecular Organic Devices. *Nature* **2002**, *420*, 800−803.
(9) Kim, T.-H.; Cho, K.-S.; Lee, E. K.; Lee, S. J.; Chae, J.; Kim, J. W.; Kim, D. H.; Kwon, J.-Y.; Amaratunga, G.; Lee, S. Y. Full-Colour Quantum Dot Displays Fabricated by Transfer Printing. *Nat. Photonics* **2011**, *5*, 176−182.
(10) Kwak, J.; Bae, W. K.; Lee, D.; Park, I.; Lim, J.; Park, M.; Cho, H.; Woo, H.; Yoon, D. Y.; Char, K. Bright and Efficient Full-Color Colloidal Quantum Dot Light-Emitting Diodes Using an Inverted Device Structure. *Nano Lett.* **2012**, *12*, 2362−2366.
(11) Bae, W. K.; Park, Y.-S.; Lim, J.; Lee, D.; Padilha, L. A.; McDaniel, H.; Robel, I.; Lee, C.; Pietryga, J. M.; Klimov, V. I. Controlling the Influence of Auger Recombination on the Performance of Quantum-Dot Light-Emitting Diodes. *Nat. Commun.* **2013**, *4*, 2661.
(12) Mashford, B. S.; Stevenson, M.; Popovic, Z.; Hamilton, C.; Zhou, Z.; Breen, C.; Steckel, J.; Bulovic, V.; Bawendi, M.; Coe-Sullivan, S. High-Efficiency Quantum-Dot Light-Emitting Devices with Enhanced Charge Injection. *Nat. Photonics* **2013**, *7*, 407−412.
(13) Dai, X.; Zhang, Z.; Jin, Y.; Niu, Y.; Cao, H.; Liang, X.; Chen, L.; Wang, J.; Peng, X. Solution-Processed, High-Performance Light-Emitting Diodes Based on Quantum Dots. *Nature* **2014**, *515*, 96−99.

DOI: 10.1021/acsnano.8b03386
ACS Nano 2018, 12, 10231−10239

(14) Lim, J.; Jeong, B. G.; Park, M.; Kim, J. K.; Pietryga, J. M.; Park, Y. S.; Klimov, V. I.; Lee, C.; Lee, D. C.; Bae, W. K. Influence of Shell Thickness on the Performance of Light-Emitting Devices Based on CdSe/$Zn_{1-X}Cd_XS$ Core/Shell Heterostructured Quantum Dots. *Adv. Mater.* **2014**, *26*, 8034−8040.
(15) Bae, W. K.; Lim, J.; Lee, D.; Park, M.; Lee, H.; Kwak, J.; Char, K.; Lee, C.; Lee, S. R/G/B/Natural White Light Thin Colloidal Quantum Dot-Based Light-Emitting Devices. *Adv. Mater.* **2014**, *26*, 6387−6393.
(16) Yang, Y.; Zheng, Y.; Cao, W.; Titov, A.; Hyvonen, J.; Manders, J. R.; Xue, J.; Holloway, P. H.; Qian, L. High-Efficiency Light-Emitting Devices Based on Quantum Dots with Tailored Nanostructures. *Nat. Photonics* **2015**, *9*, 259−266.
(17) Pal, B. N.; Ghosh, Y.; Brovelli, S.; Laocharoensuk, R.; Klimov, V. I.; Hollingsworth, J. A.; Htoon, H. 'Giant'CdSe/CdS Core/Shell Nanocrystal Quantum Dots as Efficient Electroluminescent Materials: Strong Influence of Shell Thickness on Light-Emitting Diode Performance. *Nano Lett.* **2012**, *12*, 331−336.
(18) Mueller, A. H.; Petruska, M. A.; Achermann, M.; Werder, D. J.; Akhadov, E. A.; Koleske, D. D.; Hoffbauer, M. A.; Klimov, V. I. Multicolor Light-Emitting Diodes Based on Semiconductor Nanocrystals Encapsulated in Gan Charge Injection Layers. *Nano Lett.* **2005**, *5*, 1039−1044.
(19) Bae, W. K.; Padilha, L. A.; Park, Y.-S.; McDaniel, H.; Robel, I.; Pietryga, J. M.; Klimov, V. I. Controlled Alloying of the Core−Shell Interface in CdSe/CdS Quantum Dots for Suppression of Auger Recombination. *ACS Nano* **2013**, *7*, 3411−3419.
(20) Padilha, L. A.; Robel, I.; Lee, D. C.; Nagpal, P.; Pietryga, J. M.; Klimov, V. I. Spectral Dependence of Nanocrystal Photoionization Probability: The Role of Hot-Carrier Transfer. *ACS Nano* **2011**, *5*, 5045−5055.
(21) McGuire, J. A.; Sykora, M.; Robel, I.; Padilha, L. A.; Joo, J.; Pietryga, J. M.; Klimov, V. I. Spectroscopic Signatures of Photocharging Due to Hot-Carrier Transfer in Solutions of Semiconductor Nanocrystals under Low-Intensity Ultraviolet Excitation. *ACS Nano* **2010**, *4*, 6087−6097.
(22) Klimov, V. I.; Mikhailovsky, A. A.; McBranch, D.; Leatherdale, C. A.; Bawendi, M. G. Quantization of Multiparticle Auger Rates in Semiconductor Quantum Dots. *Science* **2000**, *287*, 1011−1013.
(23) Bae, W. K.; Brovelli, S.; Klimov, V. I. Spectroscopic Insights into the Performance of Quantum Dot Light-Emitting Diodes. *MRS Bull.* **2013**, *38*, 721−730.
(24) Lannoo, M.; Delerue, C.; Allan, G. Screening in Semiconductor Nanocrystallites and Its Consequences for Porous Silicon. *Phys. Rev. Lett.* **1995**, *74*, 3415.
(25) Niquet, Y.; Delerue, C.; Allan, G.; Lannoo, M. Interpretation and Theory of Tunneling Experiments on Single Nanostructures. *Phys. Rev. B: Condens. Matter Mater. Phys.* **2002**, *65*, 165334.
(26) Schmidbauer, S.; Hohenleutner, A.; König, B. Chemical Degradation in Organic Light-Emitting Devices: Mechanisms and Implications for the Design of New Materials. *Adv. Mater.* **2013**, *25*, 2114−2129.
(27) Kondakov, D. Y. Role of Chemical Reactions of Arylamine Hole Transport Materials in Operational Degradation of Organic Light-Emitting Diodes. *J. Appl. Phys.* **2008**, *104*, 084520.
(28) Kondakov, D.; Lenhart, W.; Nichols, W. Operational Degradation of Organic Light-Emitting Diodes: Mechanism and Identification of Chemical Products. *J. Appl. Phys.* **2007**, *101*, 024512.
(29) Dong, S.-C.; Xu, L.; Tang, C. W. Chemical Degradation Mechanism of TAPC as Hole Transport Layer in Blue Phosphorescent OLED. *Org. Electron.* **2017**, *42*, 379−386.
(30) Cho, S.-Y.; Oh, N.; Nam, S.; Jiang, Y.; Shim, M. Enhanced Device Lifetime of Double-Heterojunction Nanorod Light-Emitting Diodes. *Nanoscale* **2017**, *9*, 6103−6110.
(31) Royo, M.; Climente, J. I.; Movilla, J. L.; Planelles, J. Dielectric Confinement of Excitons in Type-I and Type-II Semiconductor Nanorods. *J. Phys.: Condens. Matter* **2011**, *23*, 015301.
(32) Park, K.; Weiss, S. Design Rules for Membrane-Embedded Voltage-Sensing Nanoparticles. *Biophys. J.* **2017**, *112*, 703−713.
(33) Chang, J. H.; Hahm, D.; Char, K.; Bae, W. K. Interfacial Engineering of Core/Shell Heterostructured Nanocrystal Quantum Dots for Light-Emitting Applications. *J. Inf. Disp.* **2017**, *18*, 57−65.
(34) Caruge, J.; Halpert, J. E.; Wood, V.; Bulović, V.; Bawendi, M. Colloidal Quantum-Dot Light-Emitting Diodes with Metal-Oxide Charge Transport Layers. *Nat. Photonics* **2008**, *2*, 247.
(35) Pacholski, C.; Kornowski, A.; Weller, H. Self-Assembly of ZnO: From Nanodots to Nanorods. *Angew. Chem., Int. Ed.* **2002**, *41*, 1188−1191.

DOI: 10.1021/acsnano.8b03386
ACS Nano 2018, 12, 10231−10239